Astronomy & Astrophysics manuscript no. gbaume3293 February 2, 2008
(DOI: will be inserted by hand later)

arXiv:astro-ph/0301529v1 27 Jan 2003

Photometric study of the young open cluster NGC 3293 ⋆

G. Baume[1,2,⋆⋆], R. A. Vázquez[1,⋆⋆], G. Carraro[2] and A. Feinstein[1]

[1] Facultad de Ciencias Astronómicas y Geofísicas de la UNLP, IALP-CONICET, Paseo del Bosque s/n, 1900, La Plata, Argentina

[2] Dipartimento di Astronomia, Università di Padova, Vicolo Osservatorio 2, I-35122 Padova, Italy

Received **; accepted **

Abstract. Deep and extensive CCD photometric observations $UBV(RI)_C H_\alpha$ were carried out in the area of the open cluster NGC 3293. The new data set allows to see the entire cluster sequence down to $M_V \approx +4.5$, revealing that stars with $M_V < -2$ are evolving off the main sequence; stars with $-2 < M_V < +2$ are located on the main sequence and stars with $M_V > +2$ are placed above it. According to our analysis, the cluster distance is $d = 2750 \pm 250\ pc$ ($V_0 - M_V = 12.2 \pm 0.2$) and its nuclear age is $8 \pm 1\ Myr$. NGC 3293 contains an important fraction of pre–main sequence (PMS) stars distributed along a parallel band to the ZAMS with masses from 1 to $2.5\mathcal{M}_\odot$ and a mean contraction age of 10 Myr. This last value does not differ too much from the nuclear age estimate. Actually, if we take into account the many factors that may affect the PMS star positions onto the colour–magnitude diagram, both ages can be perfectly reconciled. The star formation rate, on the other hand, suggests that NGC 3293 stars formed surely in one single event, therefore favouring a coeval process of star formation. Besides, using the H_α data, we detected nineteen stars with signs of having H_α emission in the region of NGC 3293, giving another indication that the star formation process is still active in the region. The computed initial mass function for the cluster has a slope value $x = 1.2 \pm 0.2$, a bit flatter than the typical slope for field stars and similar to the values found for other young open clusters.

Key words. Galaxy: open clusters and associations: individual: NGC 3293 - Stars: imaging - Stars: luminosity function, mass function

1. Introduction

Star clusters constitute the most appropriate laboratory to test the stellar evolution theory since all the stars formed in a cluster belong to the same region of space, are all at the same distance and have the same chemical composition. Some of the main tools, tightly related to the history of the star formation processes, are the luminosity function (LF) and the initial mass function (IMF). Regarding the construction of these distributions, open clusters offer two operational advantages when compared to field stars: a) there is no need to assume a time-independent IMF as necessary in deriving the IMF field stars and, b) as cluster stars do not move far from their birth–sites, neither is necessary to consider the IMF is spatially independent (Scalo 1986; Herbst & Miller 1982; Wilner & Lada 1991). Still, after several years of intensive and extensive works on open clusters (in our galaxy and the Magellanic Clouds) applying the powerful CCD techniques, some questions have not found the answer yet:

- Which is the star formation mechanism and how long it keeps active (Sung et al. 1998)? Is it coeval or sequential (Iben & Talbot 1966; Herbst & Miller 1982; Adams et al. 1983)?
- Is the IMF slope universal? Is it bimodal? Why do some open clusters show an apparent deficiency of low mass stars (van den Bergh & Sher 1960; Adams et al. 1983; Lada et al. 1993; Phelps & Janes 1993; Sung et al. 1998; Prisinzano et al. 2001), despite they are young enough to exclude stellar losses by dynamical evolution?
- Does the IMF vary from cluster to cluster even within a same star formation region probably by changes in the initial conditions of the star formation process (Scalo 1986; Lada & Lada 1995)?

Send offprint requests to: gbaume@fcaglp.fcaglp.unlp.edu.ar

⋆ Based on observations collected at UTSO, ESO (Dutch 0.9 m telescope) and CASLEO. The CCD and data acquisition system at CASLEO has been partly financed by R.M. Rich through U.S. NSF Grant AST-90-15827

⋆⋆ Visiting Astronomer, CASLEO operated under agreement between CONICET of the República Argentina and the National Universities of La Plata, Córdoba and San Juan

The young open cluster NGC 3293 = C1033–579 (l = 285.9°, b = 0.07°) is placed in the Carina region north–west of Trumpler 14/16. The three clusters are embedded in the nebulosity of the HII region NGC 3372, although NGC 3293 is relatively free of patches of dust. This cluster is compact, well populated and not too much reddened. Besides, with an age $< 10\ Myr$, it is surely free from dynamical evolution too. Altogether these properties make it an excellent target to examine some of the items enumerated above. Herbst & Miller (1982, hereafter HM82) performed the deepest photometric study (mostly photographic) of this object to investigate the star–forming history down to $V \approx 15$. HM82 found features that deserve confirmation: a) the low mass stars formed first, b) the cluster LF shows a sharp dip at $M_V = +2$ and +3, c) the cluster IMF is not only flatter than the field star IMF but it varies with time during the cluster formation period and d) the cluster has a halo structure formed by less massive stars. The need for new deep photometry is evident as a substantial part of the HM82's findings may have been produced by selection effects close to the detection limit of the photographic plates (Deeg & Ninkov 1996).

Apart from the HM82 study of the star–forming history, a synthesis of the main investigations carried out in NGC 3293 includes: spectroscopy of bright cluster members to obtain radial velocities and spectral classification by Feast (1958); rotational velocity studies undertaken by Balona (1975); $UBVRI$ photoelectric photometry and polarimetric measures performed by Feinstein & Marraco (1980, hereafter FM80); UBV photometry including the cluster and the surrounding area was also carried out by Turner et al. (1980, hereafter TGHH80); important contributions including the detection of several β Cepheid stars come from $ubvyH_\beta$ observations (Shobbrook, 1980; Balona & Engelbrecht 1981, 1983; Shobbrook 1983; Balona 1994).

The present investigation aims at defining the lower main sequence structure of this cluster and detecting the presence of pre–main sequence (PMS) stars. We understand that a primary (but not concluding) indicator of the existence of PMS objects comes from the detection of faint cluster members above the ZAMS (Walker 1957, 1961). More recent evidences on PMS stars (cf. Fig. 3 in Preibisch & Zinnecker 1999) indicate that they conform a band 1^m above the ZAMS, 1 to 2^m wide approximately in the HR diagram. However, the determination of this locus through photometry alone is completely spoiled because of the contamination by field interlopers. Better defined locations are achieved by removing the field star contamination through adequate comparison fields. That implies to obtain a "clean" colour–magnitude diagram (CMD), where the PMS stars, if they do exist, occupy a well defined place. Another purpose of this investigation deals with the analysis of the frequency distribution of both, magnitudes and masses, including not only the brightest (most massive) members but also the faintest ones. Finally we will attempt to detect H_α emission stars (indicative of the PMS stage) through an $H_\alpha(on/off)$ survey that was conducted in the NGC 3293 region.

In section 2 we describe our observations, the reduction procedure and the complementary sources of information. Section 3 contains the data analysis including the estimation of the cluster angular size and the membership assignment. Section 4 illustrates the determination of the basic cluster parameters: reddening, distance, linear size and age; it also contains the cluster LF and IMF determination. Section 5 describes the process to detect stars with H_α emission. In section 6 we discuss the star formation process. Finally, the conclusions are included in section 7 along with a summary of our main findings.

2. Data Set

The main data set comes from CCD photometric observations of stars in the region of NGC 3293 carried out along several observational runs complemented with available information from the literature. Data come then from:

1. The University of Toronto Southern Observatory (UTSO): In two observational runs we obtained $UBV(RI)_C$ photometry using a PM–512 METHACROME UV coated CCD (scale $0''.45/pixel$ covering $4'$ on a side) attached to the Hellen–Sawyer 60–cm telescope. The first run was in 1994 April 13, 14 and 16 when three frames were exposed in NGC 3293 using the nitrogen–cooled detector; the second run took place in 1996 February 25 and 26, when three more frames were exposed using a glycol–refrigerated detector. Short (2 to 6 s), mid (100 to 200 s) and long (two series of up to 1100 s) exposure times were used to get photometry of the bright stars and to improve the signal–noise–ratio of the faintest stars respectively. A BV comparison frame was taken on February 27, $20'$ north of the cluster, using similar exposure times. Weather conditions at UTSO were always photometric with seeing values ranging from $1''.1$ to $1''.5$.
2. The Complejo Astronómico El Leoncito (CASLEO): In 1999 April 15 and 17 we made $V(R)_C H_\alpha$ observations in two frames ($4'.5$ radius) in the area of NGC 3293 using a nitrogen–cooled detector Tek–1024 CCD and focal reducer attached to the 215–cm telescope (scale $0''.813/pixel$). One frame was centred in the cluster and the other west side of it (see Fig. 1). Exposure times in V, $H_\alpha(on) = 656.6\ nm$ and $H_\alpha(off) = 666.0\ nm$ filters ranged from 1 s (in central frame) or 15 s (west side frame) to 700 s, and from 1 to 150 s for the R band. In all the cases, mid exposure frames were also taken.

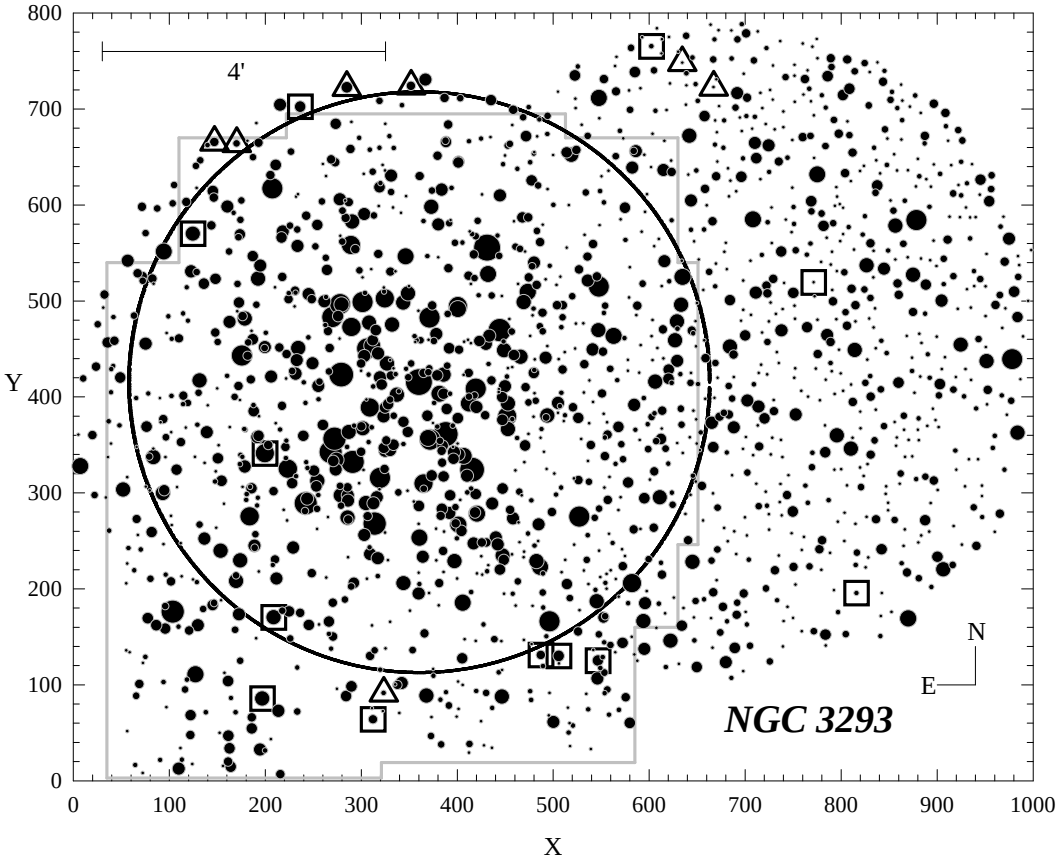

Fig. 1. Finding chart of the observed area (V filter). Black circle, $4'.1$ radius, indicates the adopted limits for the cluster from section 3.1. Grey lines indicates limits of frames from UTSO and ESO observations (that is stars with U and B measurements). For a coordinate reference, star #2 ($X = 360.3$; $Y = 415.4$), adopted as the cluster centre, has $\alpha_{2000} = 10^h\ 35^m\ 49^s.3$; $\delta_{2000} = -58°\ 13'\ 27''.4$. Stars enclosed by squares and triangles are likely and probable H_α emission stars respectively (see section 5).

3. The European Southern Observatory (ESO): We complemented our data set with an unpublished $UBV(RI)_C$ CCD photometric survey conducted by F. Patat and G. Carraro in 1996 at ESO 0.9 m Dutch telescope. Details of these observations and data reductions are given in Patat & Carraro (2001).
4. Other data sources: photometric data for a few bright stars (see Table 1) and available spectral classification were taken from FM80 and TGHH80. Useful complementary information was mainly derived from the Tycho Catalog (ESA 1997) and *SIMBAD* databases (see Tables 1 and 3).

Figure 1 shows the finding chart of all measured stars. The grey line stands for the area surveyed at UTSO and ESO ($UBV(RI)_C$) and the black circle encloses the *"cluster region"* (see section 3.1).

The reduction process was carried out using IRAF† CCDRED, DAOPHOT and PHOTCAL packages. Instrumental signatures at UTSO and CASLEO frames were removed using bias and dome flat exposures. Dark currents were tested to recognise its significance in our observations but they were found negligible. Instrumental magnitudes $UBV(RI)_C H_\alpha$ were produced via the point spread function, PSF, (Stetson 1987). Calibration sequences in the open clusters Hogg 16 and NGC 5606 (Vázquez et al. 1991, 1994) including several blue and red stars and standard star groups with blue and red stars from Landolt (1992) were used to produce final colours and magnitudes at UTSO and CASLEO respectively. The final errors of the respective calibration equations, adopted as external errors of our photometry, were < 0.025. Small mean differences < 0.03 were found between UTSO and ESO measures. However, the $V(R)_C$ measures made at CASLEO showed a shift relative to UTSO–ESO photometry that was corrected to bring them into the system defined at UTSO–ESO. The estimate of the internal errors was done comparing colour and magnitudes of the stars located in the overlapping zones of our frames. That yields typical differences < 0.03, up to $V \approx 17$. Table 1 contains the photometric output for 1690 stars; it also includes the star identification, coordinates, the cross–references with other authors and some astronomical catalogues, and the membership

† IRAF is distributed by NOAO, which are operated by AURA, under cooperatative agreement with NSF

Table 1. Photometric catalogue of the NGC 3293 region.

#	$\#_T$	$\#_{FM}$	$\#_F$	$\#_{HM}$	X	Y	V	$U-B$	$B-V$	$V-R$	$V-I$	$\Delta\ H_\alpha$	Remarks
1	3	3	3	-	431.2	555.4	6.52	-0.81	0.12	0.07 $_{FM}$	0.09 $_{FM}$	.	lm1 - HD 91943
2	4	4	4	-	360.3	415.4	6.54	-0.82	0.00	0.04 $_{FM}$	0.09 $_{FM}$	.	lm1 - HD 91969
:	:	:	:	:	:	:	:	:	:	:	:	:	:
1689	-	-	-	-	339.9	70.4	21.65 ::	.	1.12 ::	.	.	.	– - –
1690	-	-	-	-	585.0	131.4	21.72 ::	.	0.89 ::	.	.	.	– - –

Comment: Table 1 is available in full in an electronic version at the CDS. A brief summary, only indicating its structure, is shown here.

assignment. Summarising the information available after our survey we have: 1690 stars with V magnitude, 560 stars with $U-B$ index, 940 stars with $B-V$, 1550 with $V-R$, 903 with $V-I$ and 861 with $H_\alpha(on)-H_\alpha(off)$ index.

In relation to our data completeness, we performed an analysis for data from UTSO (Baume 1999) using IRAF tasks ADDSTAR, DAOFIND and ALLSTAR. Then we compared those results with ESO and CASLEO data. That analysis yielded us to the following completeness results: 100% down to $V=16$, 98.7% down to $V=17$, 94.3% down to $V=18$ and 59.2% down to $V=19$.

A comparison of our photometry with TGHH80, FM80 and HM82, in the sense "our photometry minus theirs" is shown in Table 2. The influence of (photoelectrically) unresolved stars, binary and variable stars is reflected in the large standard deviations of the mean differences. As shown in the second rows, if the known anomalous stars are discarded, the deviations decrease substantially and the mean differences and standard deviations reach acceptable values. The exception is for HM82 photometry where the bulk of their data is photographic.

3. Data Analysis

3.1. Cluster angular radius

To get reliable information on the evolutionary status of an open cluster we have to precisely know its size. In the present case, to address this issue we performed stellar counts in a $30' \times 30'$ Digitized Sky Survey (DSS) image centred in NGC 3293. All stars detected above a given threshold were assigned V_{DSS} magnitudes using DAOPHOT task. V_{DSS} magnitudes for stars brighter than $V \approx 18$ were next transformed into our photometric system with an accuracy of the order of $\pm 0.5^m$ (a procedure already applied in NGC 6231, Baume et al. 1999). Secondly, assuming the cluster is spherical, the highest apparent star density was fitted with a bi–dimensional Gaussian function. The cluster centre, defined by the highest peak (Battinelli et al. 1991), was found close to star #2 (No. 4 in FM80 notation) and the angular radius was set at $4'.1$, the distance at which the star density equalises the background level. A similar procedure but using only our CCD V data, that include stars as faint as $V \approx 20$ (Fig. 1), was applied. We counted stars inside concentric annuli, 100 pixels width, centred in star #2. As at 650 pixels of star #2, the annuli are not complete (only small portions of them were observed) we had to extrapolate the counts within each annulus to complete them. The stellar density profile coincides with the background density level at $4'.1$ from the cluster centre yielding the same result found with the DSS plates. The black circle of $4'.1$ radius shown in Fig. 1 defines then the area occupied by NGC 3293 ($''cluster\ region''$). This agrees with TGHH80's finding who yielded a cluster angular diameter of $10'$.

3.2. Cluster membership

Proper motions and radial velocities studies yield the more accurate membership determination in a cluster. Up to now, proper motions are only feasible for nearby clusters (Sanner & Geffert 2001) and radial velocities are available mostly for brightest stars. In NGC 3293, forty one of its brightest stars are listed in the Hipparcos/Tycho catalogues (ESA 1997). Only nine of them have parallax and proper motions with relative scientific value. They are indicated in Table 3 although the distance at which NGC 3293 is located makes them, statistically speaking, meaningless to derive distance and memberships. Regarding radial velocities, we used Feast (1958) studies for membership assignment to brightest stars. In particular, star #3 (No. 21 in FM80 notation) is a red super–giant ($CPD-57^\circ$ 3502; IRAS source 10338-5759) and is a likely cluster member according to its radial velocity value and its spectrophotometric distance modulus (see Table 3).

In the classical photometric method to address cluster memberships (e.g. Baume et al. 1999), the consistency of the location of each star is assessed simultaneously in all the photometric diagrams (the two colour diagram, TCD, and the different CMDs). Other authors use reddening limits within which cluster members should lie or they adopt maximum departures from a reference line as the ZAMS (Deeg & Ninkov 1996; Hillenbrand et al. 1993). Our method works well for bright members, but it becomes unpractical to detect members among faint stars in crowded fields. It was mentioned by Abt (1979) that the classical method is controversial; however, as was stated by TGHH80 and emphasised by Forbes

Table 2. Differences with previous photometric works in the sense "our photometry minus other authors"

Work	$\Delta(V)$	$\Delta(U-B)$	$\Delta(B-V)$	$\Delta(V-R)$	$\Delta(V-I)$	N
FM80	-0.06 ± 0.21	-0.01 ± 0.19	0.02 ± 0.04	-0.03 ± 0.05	-0.04 ± 0.07	(35)
	-0.01 ± 0.03	0.03 ± 0.05	0.03 ± 0.03	-0.03 ± 0.03	-0.03 ± 0.06	
TGHH80	-0.01 ± 0.10	0.01 ± 0.11	-0.00 ± 0.09			(86)
	-0.01 ± 0.06	0.01 ± 0.08	-0.00 ± 0.04			
HM82	0.04 ± 0.16	0.01 ± 0.16	0.00 ± 0.12			(278)

(1996), it is good enough when it relies on a careful inspection of the TCD and consistent reddening solutions are applied. The method works well too for nearby, not much reddened, intermediate and old clusters without traces of contracting stars (Stahler & Fletcher 1991), but it fails for young clusters where contracting stars and field interlopers very often occupy the same location on the CMD. If the reddening is high and the cluster is distant, results are clearly dubious. Therefore, in order to minimise this problem, we divided our data set in two groups, stars brighter than $V \approx 14$ and fainter than that value.

3.2.1. Bright cluster members

For stars brighter than $V \approx 14$, the method described above was combined with spectroscopic data (whenever possible) to classify stars as likely members (lm1) and probable members (pm1), which are indicated with black filled symbols in our figures. The following main features can be outlined from inspection of the cluster photometric diagrams:

- The TCD (Fig. 2a) shows, down to $B-V \approx 0.3$, a well recognisable blue and scattered main sequence composed by stars with spectral types earlier than A0 mostly included inside reddening values $0.20 < E_{B-V} < 0.45$ (see section 4.1).
- The four CMDs (Fig. 3), in turn, show a clear and well populated upper main sequence slightly widened because of differential reddening. The brightest stars of the cluster main sequence are mostly placed above the ZAMS (Schmidt–Kaler 1982) while stars with $V > 13$ are on the ZAMS.
- None of the diagrams show evidences of strong contamination of field stars among bright members. Actually, most of field stars start mixing with cluster members downwards $V \approx 12$ becoming an important obstacle to analyse the faint part of the cluster.

3.2.2. Faint cluster members

Determining memberships for stars with $V > 14$ requires a different procedure. If V vs. $B-V$ and/or V vs. $V-R$ CMDs are available for the $''cluster\ region''$ and a $''field\ region''$, we can subdivide them into a grid of boxes ($\Delta V = 1 \times \Delta(B-V) = 0.1$ and $\Delta V = 1 \times \Delta(V-R) = 0.1$) and build two–dimensional histograms for each CMD. Subtracting the respective two–dimensional histograms (this mean $''cluster\ region''$ - $''field\ region''$), we can remove (statistically speaking) the contamination produced by field stars onto the CMDs of the $''cluster\ region''$. This way, count left on the resulting two–dimensional histogram define the locus occupied by cluster member stars on the CMDs (Chen et al. 1998). Naturally, the reliability of the number of members obtained and the locus they occupy, depend on two factors: a) the adopted $''field\ region''$ must be representative of the field star distribution over the $''cluster\ region''$ and b) the $''cluster\ region''$ must include the whole extension of the cluster to account for mass segregation. Actually, the true cluster size will strongly depend on the extension of the segregation process outward it. If the $''field\ region''$ is too close to the cluster, it may contain less massive segregated members; if it is far from the cluster it may not represent the true field star distribution across it. Finally, dust clouds and emission nebulae (very frequent in young clusters near the galactic plane) along with differential reddening lead to wrong estimations of the field star distribution too (Mermilliod 1976; Prisinzano et al. 2001; see Forbes 1996 for details).

In the remaining of this section all procedures will be applied only to stars in the range $14 < V < 18$ with photometric errors < 0.1. A first point to treat is whether comparison fields around NGC 3293 do show any strong differences produced by random stellar fluctuations and/or the type of stellar data. To ease the analysis we divided our data set into four groups:

- *Sample I*: V, $B-V$ and $V-R$ data from stars placed in the cluster area, up to a $4'.1$ radius. This sample is the $''cluster\ region''$ and contains cluster stars plus field stars.
- *Sample II*: V, $B-V$ and $V-R$ data for stars placed between $4'.1$ radius and the limits of the grey line squared frames shown in Fig. 1.
- *Sample III*: V and $B-V$ data from stars placed in the comparison field (see section 2) $20'$ north of the cluster.
- *Sample IV*: V and $V-R$ data for stars from the grey line squared frames outwards.

We warn that samples II, III and IV are different representations of what we called $''field\ region''$. As they cover different areas they were adequately scaled to the $''cluster\ region''$ area to built the two-dimensional

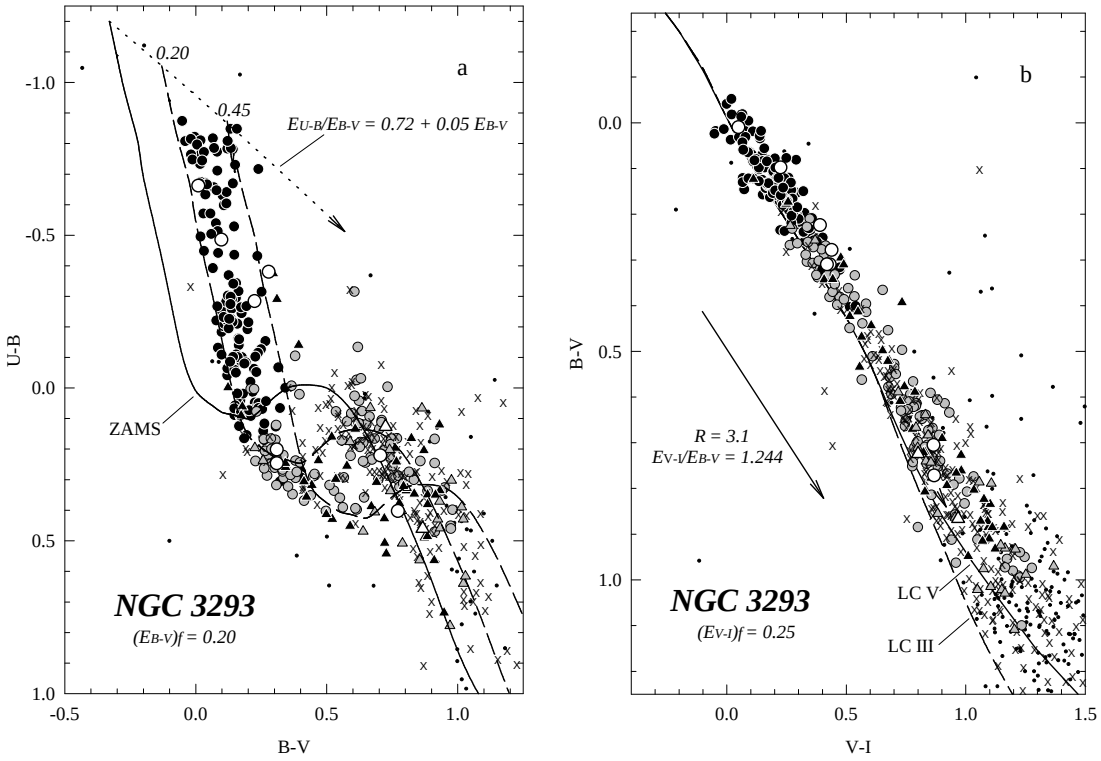

Fig. 2. a) Two colour diagram (TCD). Symbols have the following meaning: circles are likely member stars (lm) and triangles are probable member stars (pm); black symbols indicate membership obtained from the classical photometric method and grey ones those obtained from the subtraction method (see section 3.2 for explanation of the methods); crosses are non member stars (nm) and dots are stars without membership assignment; white symbols indicate likely and probable H_α emission stars (circles and triangles respectively). Solid line is the Schmidt–Kaler's (1982) ZAMS; dashed lines indicate the position of the ZAMS shifted by $E_{B-V} = 0.20$ and 0.45. Dotted arrow indicates the normal reddening path. **b)** $B-V$ vs. $V-I$ diagram. Symbols as in Fig. 2a. Solid and dashed lines are the intrinsic positions for stars of luminosity classes V and III respectively (Cousins, 1978). Solid arrow gives the normal reddening path for $R = 3.1$

histograms of each sample. Any strong spatial variation among the field samples should be revealed by the marginal distributions of the two–dimensional histograms of each sample. A brief inspection of them, shown in Fig. 4, let us say:

- Figures 4b and 4e show a same degree of completeness of the photometry in the $''cluster\ region''$ and the field samples down to $V \approx 18$.
- Figs. 4a-c, show that different field samples have not only the same shape (down to $V \approx 18$) but also the same number of stars approximately. Aside from uncertainties produced by small number statistics, the actual true distribution of field stars over the cluster surface should not differ too much from these three.

To quantify the last issue, we applied a Kolmogorov–Smirnoff test to the field distributions confirming that, for $V < 18$, the three field samples are similar at the level $\alpha = 0.05$. Thus, the average of their respective two–dimensional histograms (V vs. $B-V$ and/or V vs. $V-R$) yields the best representation of the $''field\ region''$ across NGC 3293. The corresponding marginal distributions are presented as white histograms in Figs. 4d-f).

Another point to analyse is whether NGC 3293 has undergone mass segregation and shows a core/halo structure, as suggested by HM82. Although in section 3.1 we did not find evidences of any halo around NGC 3293, we compared the ratios of stellar densities found in the $''cluster\ region''$ (ρ_{IN}) and outside it (ρ_{OUT}) as a function of V. If an appreciable amount of less massive (faint) stars were located outside the cluster boundaries due to an active mass segregation process then the ρ_{OUT}/ρ_{IN} ratio should show that. As expected, the plots of Fig. 5 do not indicate any appreciable star over excess outside the cluster area, but just a very slow increasing at very faint magnitudes (at the level where the completeness starts being questionable). We conclude that the cluster has not undergone mass segregation and its limits from section 3.1 are fully reliable.

We proceeded then to subtract the average two–dimensional histogram of the $''field\ region''$ from the one of the $''cluster\ region''$ obtaining the contamination–free V vs. $B-V$ and V vs. $V-R$ distributions. They revealed

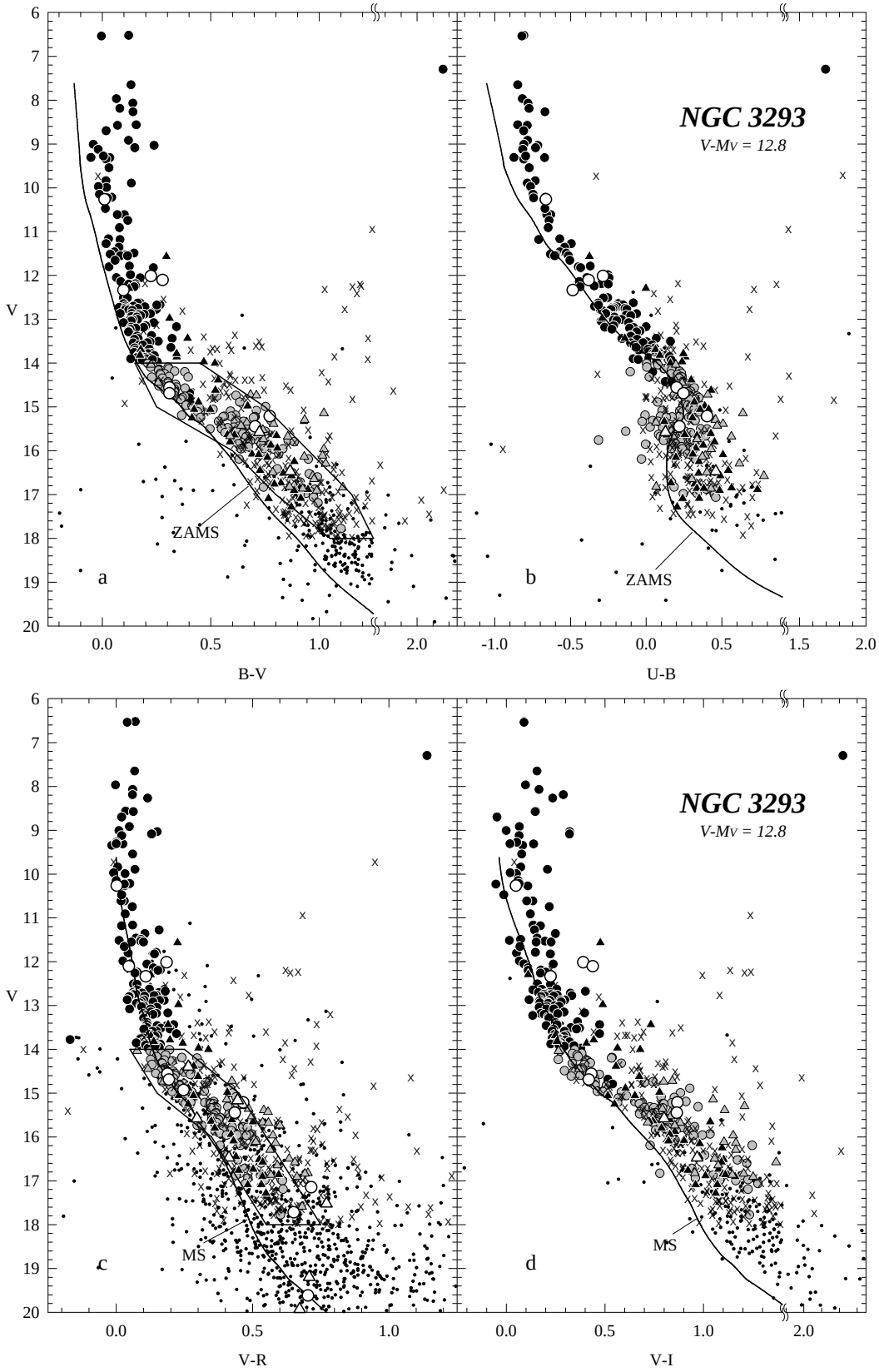

Fig. 3. Colour–magnitude diagrams (CMDs). Symbols as in Fig 2a. Solid line in **a** and **b** is the Schmidt–Kaler's (1982) ZAMS and the Cousins' (1978) intrinsic line for luminosity class V stars in **c** and **d** fitted to the apparent distance modulus $V - M_V = 12.8$ ($V - M_V = V_0 - M_V + R\ (E_{B-V})_f$, see sections 4.1 and 4.2). Closed curves in **a** and **c** indicate limits adopted for faint stars membership (see section 3.2.2).

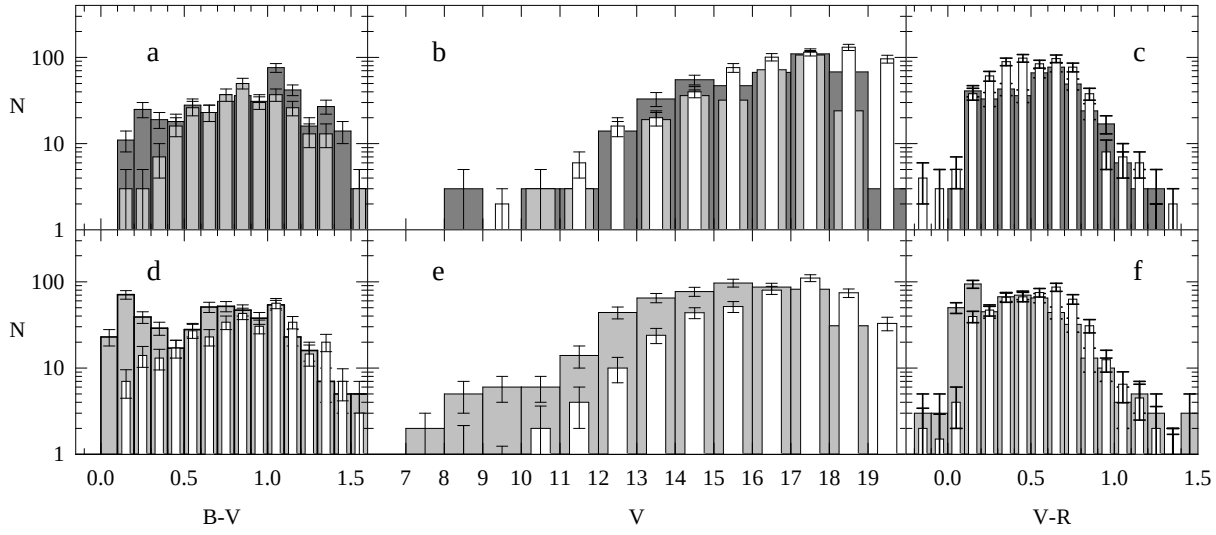

Fig. 4. Marginal distributions of the two–dimensional histograms of the different samples taken from our data (see section 3.2.2). Upper panels, **a**,**b** and **c**, represent what we call $''field\ regions''$: dark–grey distributions belong to *Sample II*, grey ones to *Sample III* and white ones to *Sample IV*. In **d**, **e** and **f**, grey distributions belong to *Sample I* ($''cluster\ region''$ containing cluster plus field stars) while the white ones stand now for the average of samples *II*, *III* and *IV* (our best representation of the $''field\ region''$

then the presence of stellar bands above the ZAMS with confident lower and upper limits. Such limits were used on the CMDs (see Figs. 3a and 3c) to define which stars are (from a statistical point of view) cluster members following the next criteria:

- A star is a cluster likely member (lm2) if it is found inside the cluster boundaries defined in section 3.1 and is simultaneously included inside the band limits in the two CMDs (V vs. $B-V$ and V vs. $V-R$).
- A star is a probable member (pm2) if, apart from being spatially well located, it fits, at least, in any of high density zones defined in the CMDs and shows slight departures in the other.

Finally, the resulting sample was filtered (following a random distribution) in order to obtain final CMDs with an amount of stars in each colour–magnitude box similar to that obtained after the subtraction of the two–dimensional histograms. The adopted memberships are shown with grey filled symbols in the photometric diagrams of our figures. Notice in advance member stars with $V > 15.5$ mainly placed above the ZAMS line in the V vs. $B-V$ and V vs. $V-I$ diagrams (we will return to this point in subsection 4.3 and section 6).

4. Cluster Parameters

4.1. Corrected colours and magnitudes of cluster members

For the estimation of the cluster mean colour excesses, we used firstly the 14 stars with known spectral classification and luminosity class IV–V (see Table 3) using the Schmidt–Kaler (1982) relations of spectral types and intrinsic colours (Be stars were excluded). The plot of excesses is shown in Fig. 6a together with the standard E_{U-B}/E_{B-V} relation. The fitting is poor probably because of colour anomalies of the many variable stars present in the sample. Mean value excesses of these stars were $E_{B-V} = 0.29 \pm 0.06$ $(s.d.)$ and $E_{U-B} = 0.23 \pm 0.08$ $(s.d.)$. Secondly, we applied the well known relations $E_{U-B}/E_{B-V} = 0.72 + 0.05\ E_{B-V}$ and $(U-B)_0 = 3.69\ (B-V)_0 + 0.03$ to get the intrinsic colours of those stars with $V < 14$ adopted as likely members and without spectral classification (mostly located at $0.20 < E_{B-V} < 0.45$, see Fig. 2a). When we included this last group of stars in the mean colour excesses computations, the obtained values were $E_{B-V} = 0.29 \pm 0.06$ $(s.d.)$ and $E_{U-B} = 0.21 \pm 0.05$ $(s.d.)$, almost identical to the obtained firstly. We de-reddened cluster members with $V < 14$ (except star #3) using individual excesses, meanwhile other cluster members and star #3 were de-reddened using these lasts mean

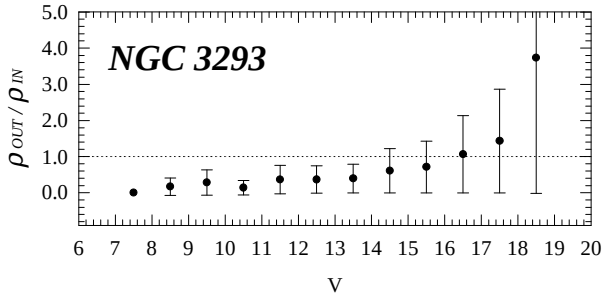

Fig. 5. ρ_{OUT}/ρ_{IN} vs. V diagram. Poisson statistic error in each magnitude are also indicated.

excess values. The estimated foreground colour excesses of NGC 3293 were $(E_{B-V})_f = 0.20$ and $(E_{U-B})_f = 0.15$, slightly lower than the typical ones for southern Carina (Tr 15, Carraro 2002; Tr 14/15/16, Tapia et al. 2002).

The next step was to know the absorption law valid in NGC 3293 given by $R = A_V/E_{B-V}$. Galactic regions with normal absorption have a mean of $R = 3.1 - 3.2$ although larger R–values are especially found in regions of recent star formation. To compute the local R–value we obtained individual E_{B-V}, E_{V-R} and E_{V-I} excesses through the $(B-V)_0$ with $(V-R)_0$ and $(V-I)_0$ relations for stars without spectral classification (circles in Fig. 6b-c) and the relation between MK types and $(V-R)_0$ and $(V-I)_0$ for stars with spectral types (squares in Fig. 6b-c), both from Cousins (1978). E_{V-R}/E_{B-V} and E_{V-I}/E_{B-V} ratios depend on the R_V–values as when $E_{V-R}/E_{B-V} = 0.57$ and $E_{V-I}/E_{B-V} = 1.244$ the interstellar material is normal (Vázquez et al. 1995; Dean et al. 1978). The plot of 140 stars with E_{B-V}, E_{V-R} and E_{V-I} are depicted in Figs. 6b and 6c showing an excellent agreement with the typical reddening relations. The mean ratios found are $E_{V-R}/E_{B-V} = 0.54 \pm 0.15$ $(s.d.)$ and $E_{V-I}/E_{B-V} = 1.26 \pm 0.18$ $(s.d.)$, indicative of a normal reddening law for which is $R = 3.1$. The foreground excesses we found were $(E_{V-I})_f = 0.25$ and $(E_{V-R})_f = 0.11$. Finally we mention that FM80 claim that R can raise up to 3.5. That is marginally probable seeing the plots of Fig. 6b-c, although the scatter around the mean lines may be mainly caused by circumstellar envelopes, variability and/or binarity instead of anomalies in the absorption. Therefore, we adopted $R = 3.1$ to obtain corrected magnitudes as $V_0 = V - 3.1\ E_{B-V}$.

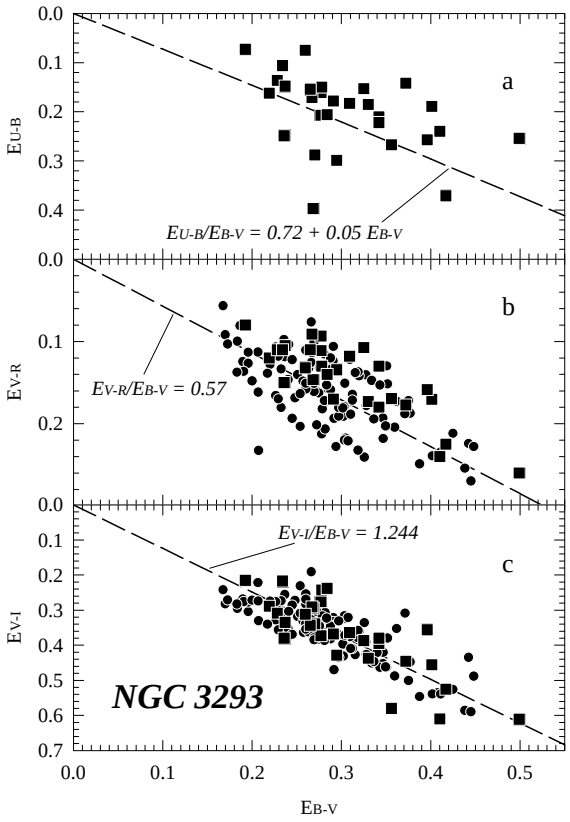

Fig. 6. E_{U-B}, E_{V-R} and E_{V-I} vs. E_{B-V} diagrams for likely cluster members with $V < 14$ except star #3 and Be stars. Squares are stars with available spectral classification and dashed curves indicate normal relations.

4.2. Cluster distance and size

The distance of NGC 3293 was derived superposing the Schmidt–Kaler's (1982) ZAMS onto the reddening–free CMD. The best ZAMS fitting was achieved for a distance modulus $V_0 - M_V = 12.2 \pm 0.2$ (error from eye–inspection). We also applied the spectroscopic parallax method to 33 stars to get the cluster distance modulus (using the relation of spectral types and M_V from Schmidt–Kaler 1982) that yielded 12.1 ± 0.5. If only 17 stars of luminosity class IV–V are used, the distance modulus turns out to be 12.3 ± 0.5 (see last column in Table 3). The large dispersions of the moduli associated to the spectroscopic parallax method may be intrinsic for early type stars (Conti & Underhill 1988) or produced by a high percentage of variable and binary stars (Feast, 1958). Our distance modulus is a bit larger than the ones given by Feast (1958), 12.08 ± 0.1, FM80, 12.1 ± 0.15, TGHH80 11.99 ± 0.13, Shobbrook (1983), 11.95 ± 0.1 and lesser than the one from Balona & Crampton (1974), 12.32 ± 0.09. Notwithstanding, as at 1σ, all of them are almost coincident, we adopted $V_0 - M_V = 12.2 \pm 0.2$ which yields a cluster distance $d = 2750 \pm 250$ *pc*. The absolute magnitude scale M_V shown in Fig. 7 was set with this mean value.

When the above distance modulus is combined with the angular radius obtained in section 3.1 it yields a linear cluster radius 3.3 ± 0.3 *pc*, comparable to the sizes of other studied young open clusters as Cr 272, 4.0 *pc*; NGC 6231, 4.1 *pc*, and H-M 1, 2.9 *pc* (from Vázquez et al. 1997; Baume et al. 1999 and Vázquez & Baume 2001 respectively). This result however disagrees with the Janes et al. (1988) result that most of young clusters have diameters less than 5 *pc*.

4.3. Cluster age

4.3.1. Nuclear age

Regarding the nuclear age of NGC 3293, the isochrones derived from Girardi et al. (2000) evolutionary models (computed with solar metallicity, mass loss and overshooting) are shown in Fig. 7a-b superposed to the cluster upper main sequence. Because an important fraction of bright members were de–reddened using their spectral types some scatter arises that precludes a single

Table 3. Main characteristics of bright stars in NGC 3293

#	$\#_{FM}$	ST	Remarks	E_{B-V}	E_{U-B}	E_{V-R}	E_{V-I}	$V_o - M_V$
1	3	B0..5 Iab	V513 Car - Hip-Tyc -	0.34	0.22	0.18	0.38	11.86
2	4	B0 Ib	- Hip-Tyc -	0.24	0.25	0.15	0.38	11.91
3	21	M1.5 Iab	V361 Car - IRAS -					12.00
4	22	B1 II	- - s.d.s.	0.37	0.14	0.18	0.45	11.90
5	20	B1 III	V439 Car - -	0.33	0.15	0.11	0.39	11.36
6	25	B1 III	- -	0.40	0.19	0.17	0.46	11.23
7	6	B0.5 III	- -	0.36	0.27	0.17	0.58	11.84
8	8	B0.5 III	- Hip-Tyc -	0.42	0.37	0.23	0.53	11.72
9	26	B1 III	V379 Car - - Be(3) - βCeph	0.42	0.12	0.14	0.44	11.67
10	7	B1 III	- - b.s.(1)	0.33	0.19	0.17	0.44	11.95
11	16	B1 IV	V403 Car - - βCeph	0.28	0.15	0.13	0.24	11.44
12	27	B0.5 III	V380 Car - - βCeph	0.40	0.26	0.16	0.36	12.44
13	5	B1 III	V381 Car - - βCeph - b.s.(1)	0.22	0.16	0.12	0.29	12.73
14	19	B1 III	- - s.d.s.	0.50	0.25	0.26	0.61	11.89
15	2	B1 III	- Hyp-Tyc -	0.41	0.24	0.24	0.61	12.22
17	18	B1 V	V406 Car - - βCeph	0.27	0.15	0.11	0.34	11.65
18	14	B0.5 V	V405 Car - - βCeph	0.23	0.14	0.11	0.31	12.20
19	24	B1 III	V378 Car - - βCeph	0.29	0.30	0.13	0.43	12.80
20	23	B1 III	V404 Car - - βCeph - s.d.s.	0.28	0.16	0.09	0.37	12.89
21	10	B1 V	V401 Car - - βCeph	0.29	0.18	0.17	0.37	11.84
22	43	K5	- Hip-Tyc - r.fg.s.					
23	42	A0	- Hip-Tyc -					
25	12	B1 V	V402 Car - - Be(2) - b.s.(1)	0.39	0.16	0.18	0.50	12.77
27	9	B2 V	- Hip-Tyc - b.s.(1)	0.26	0.07	0.13	0.31	11.59
28	13	B1.5 V	- -	0.24	0.15	0.10	0.34	12.22
30	15	B1 V	- - s.d.s.	0.28	0.21	0.14	0.24	12.55
31	28	B1 V	- - H_α - b.s.(1)	0.27	0.29	0.11	0.34	12.63
33	17	B2.5 V	V440 Car - -	0.23	0.11	0.11	0.22	11.75
34	33	B2 V	- -	0.34	0.21	0.13	0.40	11.95
35	29	B2 V	- -	0.31	0.18	0.12	0.36	12.06
38	-	B8	- Hip-Tyc - b.bg.s.					
47	31	B2 V	- -	0.28	0.21	0.11	0.28	13.06
48	-		- Hip-Tyc -					
96	30	B5 V	- -	0.27	0.40	0.15	0.29	13.01
115	35	B7 V	- -	0.27	0.17	0.09	0.29	12.64
116	34	B8 V	- -	0.19	0.07	0.08	0.22	12.47
120	32	B8 V	- - Be(1)	0.19	0.21	0.13	0.27	12.50

Remarks:
b.s. = binary star
s.d.s. = star in double system
r.fg.s. = red foreground star
b.bg.s. = blue background star
βCeph = beta cepheid star
H_α = likely H_α emission star
Be = Be star
IRAS = Source IRAS 10338-5756
Hip-Tyc = Star with paralax and proper motion measurements (see Table 1 for HIP/TYC identification)
(1) = Feast (1958); (2) = Schild (1970); (3) = Shobbrook (1980)

Notes:
- $\#_{FM}$ indicates numbering from FM80.
- Spectral classification was taken from TGHH80 and FM80.
- $V_0 - M_V$ column contains spectrophotometric distance moduli.
- Remarks information is mainly from *SIMBAD* database.

isochrone to fit the bright part of NGC 3293; binaries and fast rotators are likely to be another source of scatter in upper CMD. The envelope of binaries 0.75^m above the ZAMS encloses pretty well most of binary stars in the upper main sequence. We draw the attention on the red super–giant (star #3) which is not included by any isochrone (Fig. 7a), but it lies close to the isochrones of $10 - 12.6\ Myr$. As many other red–supergiant stars, this star is not contained by any isochrone, a frequent effect already reported in Meynet et al. (1993).

From stars with $M_V < -4$, the nuclear age of NGC 3293 goes from 6.5 to 10.0 Myr with a probable mean age of 8 Myr. The cluster is thus older than in previous investigations, $5 \pm 2\ Myr$ by TGHH80 and $6 \pm 2\ Myr$ from HM82. Such differences may have their origin in different (smaller) distance moduli estimates and also in the use of different isochrone sets.

4.3.2. Contraction age

As indicated in section 3.2.2, a relevant feature emerging from the cluster lower sequence (Fig. 7c) is that the left envelope of NGC 3293 does not follow the shape of the ZAMS. The lower cluster sequence shows a bend at $M_V \approx +2$, lower of which it lies 1^m above the ZAMS approximately constituting a parallel sequence that confirms the earlier assertion of HM82 that faint

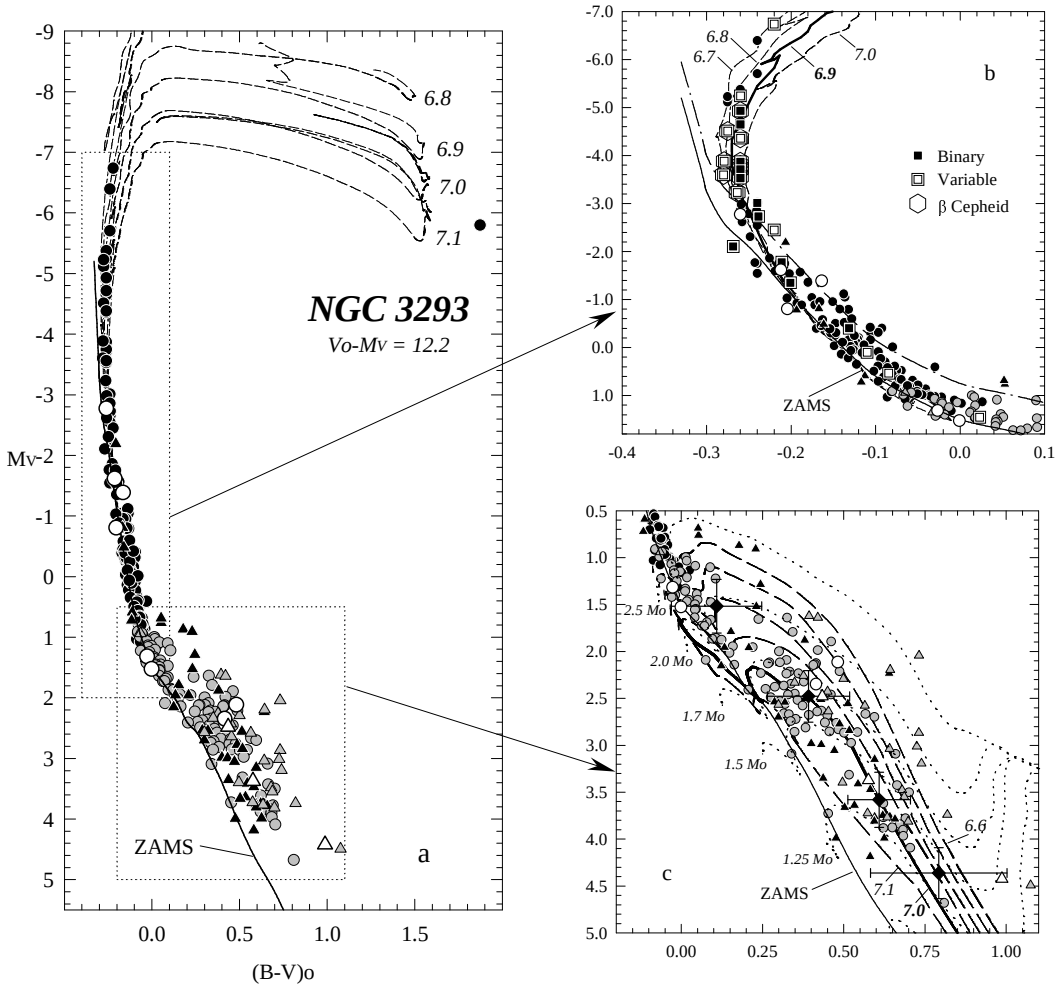

Fig. 7. a) The entire M_V vs. $(B-V)_0$ diagram. Symbols as in Fig. 2a. Solid line is the Schmidt–Kaler's (1982) ZAMS. Dashed lines are the isochrones from Girardi et al. (2000). Numbers give the $\log age$. **b)** An enlargement of the upper main sequence showing the binary envelope (dotted – dashed line) 0.75^m above the ZAMS. The thick line is the isochrone of 8 Myr. Numbers as in **a**. **c)** An enlargement showing the faint sequence of the cluster. Dotted and dashed lines represent the tracks and isochrones (Bernasconi & Maeder 1996). Numbers indicate the masses of each track and the $\log(age)$. The 10 Myr isochrone is shown as a thick line. Mean values and dispersions of PMS stars grouped at intervals $\Delta M_V = 1$ are also indicated

stars are mostly above the ZAMS.

As contamination of field interlopers has been already removed, the stars in this parallel sequence have to be interpreted as stars in contraction phase towards the ZAMS. The strong M_V scatter at constant colour is a normal feature associated to the age spread (Iben & Talbot 1966) among these type of objects (cf. Fig. 3 in Preibisch & Zinnecker 1999). However, the contrast between the wide PMS band and the sharp upper main sequence in Fig. 7c is produced primarily by: a) differential reddening, that was not removed from the main sequence faint stars (they were de–reddened using the mean excess values derived in section 4.1) and, b) several intrinsic factors detailed below. In overlaying in Fig. 7c the accretion evolutionary models developed by Bernasconi & Maeder (1996) we find that the PMS objects have masses ranging from 1 to $2.5\mathcal{M}_\odot$ and ages from 6 to 12 Myr, a PMS age range close to ~ 5 Myr found recently in the other Carina clusters Tr 14, Tr 15 and Tr 16 by Tapia et al. (2002) and confirmed in Tr 15 by Carraro (2002).

We do not find a single isochrone that fits the whole lower sequence; indeed PMS stars tend to cross several of them. This lack of alignment led Iben & Talbot (1966) to reject out the hypothesis of coeval star formation in the clusters NGC 2264 and NGC 6530. Recently, the same was done in NGC 2264 by Flaccomio et al. (1999). Notwithstanding, departures from a single isochrone produced by differential reddening, binarity/multiplicity, random distribution of accretion discs around single and multiple systems, photometric errors and physical uncertainties in the evolutionary models are expected to

happen. The influence of differential reddening is hard to estimate as it affects in different manners different stars. As for binarity, it is very frequent not only among normal less massive stars (> 50%, Bessell & Stringfellow 1993; Preibisch & Zinnecker 1999) but also among PMS stars (Hartigan et al. 1994). Binarity raises the stars above a reference line (e.g. the ZAMS) in a way that depends on the mass ratio of the binaries. As for the accretion stellar discs, their occultation and emission, and also the random orientation of their angles, coupled with a possible range of accretion rates (Kenyon & Hartmann 1990) introduce more scatter among the PMS population.

To smooth these effects, the mean of the stellar distribution in Fig. 7c was computed. Interestingly, the mean follows closely the isochrone of 10 Myr shown by a thick line, except at $M_V = +1.5$. This is a magnitude point where very often (Rachford & Canterna 2000, Phelps & Janes 1993; de Bruijne et al. 2000) a gap appears in many open clusters so that the statistics here may be irrelevant. Therefore we adopt 10 Myr as the mean contraction age of the PMS population in NGC 3293.

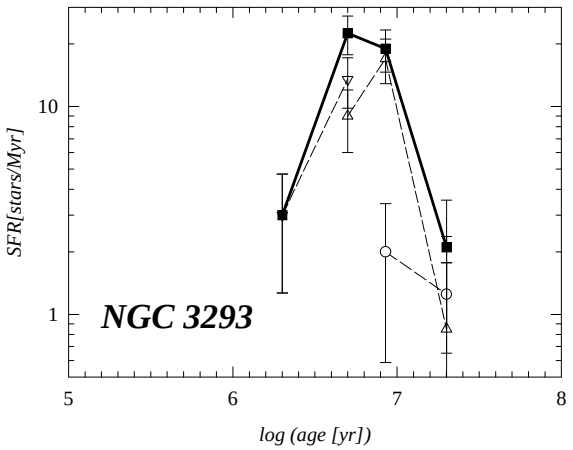

Fig. 8. Star formation rate (SFR) in NGC 3293 from Bernasconi & Maeder (1996) evolutionary models. Circles, upside triangles and downside triangles indicate SFR values for stars with masses in the intervals $1.0-1.5$, $1.5-2.0$ and $2.0-2.5\mathcal{M}_{\odot}$ respectively. Thick line (black squares) represents the total SFR. Error bars are from Poisson statistic.

4.3.3. Star formation rate

Does the fact of finding a 6 Myr age spread among PMS objects indicate the star formation process is not coeval? We examined the point computing individual present–day masses of PMS stars and giving them the corresponding ages interpolating among Bernasconi & Maeder (1996) models. Following Iben & Talbot (1966) and Adams et al. (1983) definitions and procedures, we estimated the star formation rate (SFR) in the cluster for three different stellar masses bins. The results, shown in Fig. 8, suggest no dependence of the SFR with stellar masses when allowing for the uncertainties involved in that kind of computation (see Stahler 1985). Actually it seems to confirm that the stellar formation in NGC 3293 took place in a very short period of time, mostly between 7 and 10 Myr ago.

4.3.4. Nuclear and contraction ages

The mean contraction age of the entire PMS population becomes comparable to the mean nuclear age deduced from stars with $M_V < -4$ since there is no substantial difference between the 8 Myr and 10 Myr ages of evolved and PMS stars respectively. Most important is that the early original age discrepancy of 20 Myr found by HM82 is now strongly reduced. On the other hand, as mentioned above, companion stars (Preibisch & Zinnecker 1999) overestimate the luminosity of a given star (e.g., underestimating the luminosity of an M0 star by a factor of 2 reduces its age by a factor of 4 and for a factor of 2 for a G5 star). Also, the net effect of accretion stellar discs, as was mentioned above, introduce scatter in luminosities that produce uncertainties of a factor of $2-3$ in the age of an individual object (Kenyon & Hartmann 1990). We are confident therefore, that the 2 Myr difference found between the mean contraction age and the nuclear age, results irrelevant in view of the mentioned effects.

Moreover, the 0.2^m error of the distance modulus can reduce or increase the difference between both ages without affecting the nuclear age which remains almost invariable. Besides, the "turn on" point position (see Fig. 7c) is not very accurately determined but, allowing for the above uncertainties, it can be placed at $M_V \approx +2$ corresponding to a stellar mass $\sim 2\mathcal{M}_{\odot}$ with a contraction age of 7.9 Myr close to the nuclear age.

4.4. Cluster LF and IMF

4.4.1. The Luminosity Function

The cluster LF gives the fraction of stars in each absolute magnitude bin of size $\Delta M_V = 1$. The grey histogram in Fig. 9 shows the LF of NGC 3293 where known cluster binaries (see Table 3) were all corrected by 0.75 and two stars were counted instead of one. For comparison purposes we included also the cluster LF earlier determined by HM82 and the cluster overall LF found by Phelps & Janes (1993). Except by the strong dip present at $M_V = -2$ in the HM82 LF, there is no important differences among the three LFs down to $M_V \approx +1$. From $M_V \approx +1$, HM82 LF differs from ours as the sharp dip at $M_V \approx +3$ is not revealed by our data. Somehow, that confirms the suspicion of HM82

that the dip they found is an artifact produced by a combination of incompleteness and eye-estimate of field faint star magnitudes. Interesting enough, our LF as well as the HM82's show an apparent low number of stars for $M_V > 0$ when comparing with the Phelps & Janes estimation: ours, in particular, shows a flattening in the range $0 < M_V < +3 - +4$. At this point it is necessary to notice that all stars below $M_V \approx +2$ are PMS objects as we have already stated and their luminosities do not represent the luminosities they will have in the ZAMS; depending on the star location, the present star luminosity and the final in the ZAMS will differ for more than 1^m changing the LF shape. Therefore, the cluster LF is only comparable to another from main sequence objects (Wilner & Lada, 1991) in the range $-7 < M_V < +2$.

4.4.2. The Initial Mass Function

Stellar masses were derived using an interpolation process (Baume et al 1994) converting the M_V, $(B-V)_0$ and $(U-B)_0$ values into $\log L$ and $\log T_{eff}$ first, where a mass is assigned in this theoretical plane. The code uses bolometric corrections from Schmidt-Kaler and interpolates among evolutionary tracks reconstructing the path of a given star backwards to its original point in the ZAMS. Bernasconi & Maeder (1996) tracks were used for masses $< 2.5\mathcal{M}_\odot$ and Girardi et al. (2000) tracks for stars above that mass limit. Appropriate mass bins were adopted to distribute stellar masses as shown in Table 4 and the mass points are depicted on top of Fig. 10 with the $\sqrt{N}$ count bars. To get the slope of the cluster IMF (x) we used a weighted least squares method applied to different mass ranges whose results are included at bottom of Table 4. The lowest mass bin has been excluded of any calculations as it may be affected by effects described below. The fitting of the most massive stars gives a steep slope with a high error value ($x = 1.6 \pm 0.5$), however the portion that includes low and intermediate mass stars yields a flatter slope ($x = 1.2 \pm 0.2$). The last value is closer to the typical slope for field stars ($x = 1.35$) and only marginally comparable to the $x = 0.9$ found by HM82.

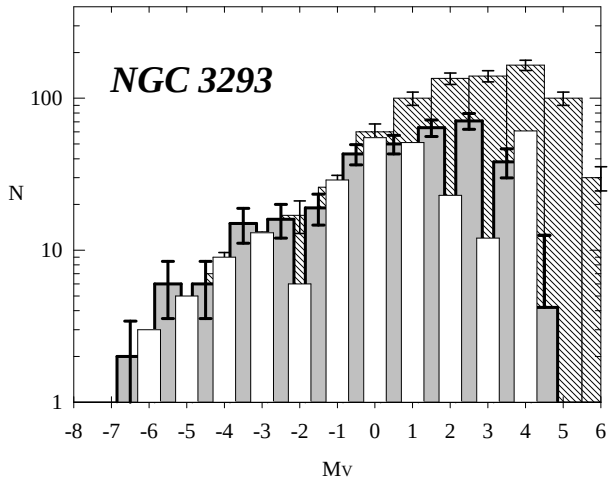

Fig. 9. Luminosity Function of NGC 3293 (grey histogram). Error bars are from Poisson statistic and the sustraction process. The white histogram is the LF from HM82 and the hatched one is the combined LF of several young open clusters from Phelps & Janes (1993).

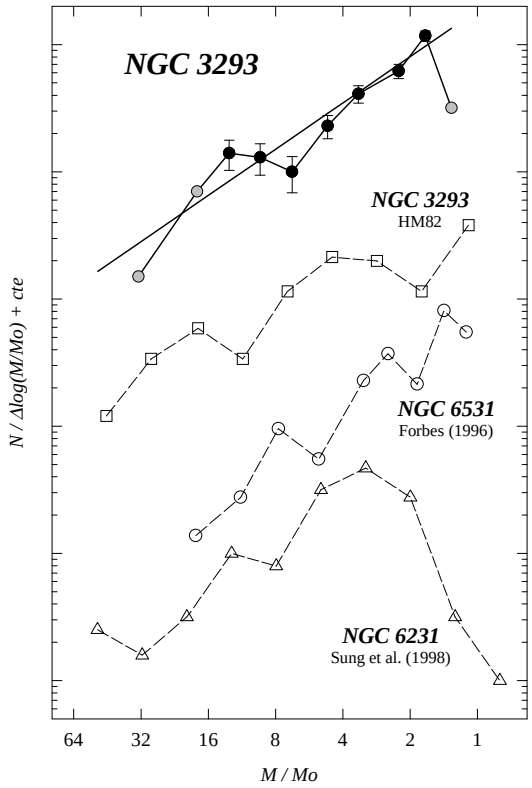

Fig. 10. Initial Mass Function (IMF). The IMF obtained for NGC 3293 is shown at the top (error bars are from Poisson statistic). The weighted least square fitting for the mass range $1.41 < \mathcal{M}/\mathcal{M}_\odot < 16.0$ is also presented (points not included in the fit are indicated with grey symbols). Other IMFs for comparable clusters are also shown.

Figure 10 also includes IMFs of cluster of similar ages and the earlier IMF of NGC 3293 determination made by HM82. Interesting common features are shown by the three clusters in the figure. There is always an increasing star number till a dip or flat zone appears. The mass range of the dip is not the same in the three clusters. While ours happens at $8\mathcal{M}_\odot$, it happens at $10\mathcal{M}_\odot$ in the HM82 IMF. Coincident with ours is the dip at $8\mathcal{M}_\odot$ in NGC 6231 but the most strange location corresponds to the IMF of NGC 6531 whose dip happens at $6\mathcal{M}_\odot$. The pattern is not easy to explain but the differences in the mass may reflect differences in the method of assigning masses on the ZAMS according to the evolutionary models used.

Table 4. The Initial Mass Function.

$\Delta\mathcal{M}/\mathcal{M}_\odot$	$\Delta M_V^{(a)}$	$N^{(b)}/\Delta\log(\mathcal{M}/\mathcal{M}_\odot)$
$22.63 - 45.25$	$-7.0 - -6.0$	1.5 ± 1.2
$16.00 - 22.63$	$-6.0 - -4.2$	7.0 ± 2.6
$11.31 - 16.00$	$-4.2 - -3.1$	14.0 ± 3.7
$8.00 - 11.31$	$-3.1 - -2.2$	13.0 ± 3.6
$5.66 - 8.00$	$-2.2 - -1.3$	10.0 ± 3.2
$4.00 - 5.66$	$-1.3 - -0.5$	23.0 ± 4.8
$2.83 - 4.00$	$-0.5 - +0.4$	41.0 ± 6.4
$2.00 - 2.83$	$+0.4 - +1.6$	62.0 ± 8.0
$1.41 - 2.00$	$+1.6 - +3.3$	117.0 ± 10.8
$1.00 - 1.41$	$+3.3 - +5.0$	31.8 ± 8.3
$\Delta\mathcal{M}/\mathcal{M}_\odot$	x	
$1.41 - 45.25$	-1.23 ± 0.13	
$1.41 - 16.00$	-1.21 ± 0.18	
$8.00 - 45.25$	-1.63 ± 0.52	

Notes: (a) Approximated values valid for the evolutionary status of NGC 3293. (b) Known binaries and incompleteness effects were considered.

4.4.3. Uncertainties in the LF and the IMF

There are three main sources of uncertainties in the determination of both, the LF and the IMF: the field star correction, the incompleteness of the photometry and the unresolved binaries. Other effects of course do contribute, but the mentioned are the most difficult to assess. As for the removal of the star field contamination we are confident on the goodness of our method and the choice of the areas. Incompleteness is a bit more complex phenomenon to quantify. An analysis of the completeness factors was presented in section 2 and to remove in part this effect, we applied those factors to the amount of stars in each bin of our LF. However, our conclusions may still be affected for incompleteness at the lowest luminosity bin. This uncertainty was minimised in our estimation of the LF that was set in the range from -7 to $+2$ and was also minimised in the computation of the IMF by excluding the lowest mass bin. Unresolved binaries, however, may influence the entire mass range. We will just describe the probable effect on our determination as the issue has been treated by many worker and detailed calculation have been already performed. Under the hypothesis that stellar masses of binary components are randomly distributed Sagar & Richtler (1991) studied the mass range $2 - 14\mathcal{M}_\odot$ finding that, if a fraction of 50% binaries is present in a given cluster, its IMF slope undergoes a flattening of 0.2 for an initial slope of 1.5. Lower initial slopes are less flattened according to these authors. Another analysis made by Kroupa et al. (1991, 1992) and Kroupa & Gilmore (1992) also dealt with the point reaching the conclusion that if a Salpeter model is assumed, results lead to an apparent deficiency of low mass stars. This effect is probably the one producing the apparent deficiency of stars in the LF of NGC 3293 when compared to the overall LF of Phelps & Janes (as marginally shown in Fig 9).

5. The search for stars with $H\alpha$ emission

One of the aims of this work is the detection of stars with H_α emission. To assess whether a star shows H_α emission, we used the $H_\alpha(on) - H_\alpha(off)$ (hereafter $\Delta\ H_\alpha$) index. Similar indices has been already used in other works (Adams et al. 1983; Sung et al. 1998). We want to mention that due to poor weather conditions, the seeing during the exposures of H_α frames was large ($2'' - 2''.5$) producing distortions in the final photometry of the stars, especially those with close companions. That, probably, yielded the high errors generated by DAOPHOT, especially in the $H_\alpha(off)$ frames.

Figure 11b shows the histogram (white) of $\Delta\ H_\alpha$ values including all stars. The hatched one contains only stars with errors < 0.10 and was fitted with a Gaussian distribution function over the interval $-0.5 < \Delta H_\alpha < 0.9$ with mean value $\langle\Delta H_\alpha\rangle = 0.21$ and standard deviation $\sigma_{\Delta H_\alpha} = 0.18$. The mean value, which is assumed to correspond to non–emission objects, is close to the values found by Adams et al. (1983) in NGC 2264 (0.30) and NGC 7089 (0.23). However, the dispersion among our data is over twice the value 0.08 found in NGC 2264 by them. Following Adams et al. reasoning, we identify a probable H_α emission star when its index value is $\Delta H_\alpha < -0.34$ (further than 3σ from the mean value) and a likely emission star if it is $\Delta H_\alpha < -0.50$ (further than 4σ). All stars showing evidences of emission were plotted with white symbols in the photometric diagrams. It is interesting to mention the clear separation of stars with H_α emission when ΔH_α values are plotted against the $V - R$ index (see Fig. 11a). We are aware that this procedure only detect stars with high H_α emission while most of PMS stars show weak H_α emission making their detection much harder (Preibisch & Zinnecker 1999).

Nineteen stars, listed in Table 5, show evidences of having H_α emission. Their spatial locations in the NGC 3293 area (shown in Fig. 1) is interesting as eleven of them lie in the external border of the cluster and just another three are inside the cluster limits. From the spatial point of view there is no concentration of emission stars towards the cluster centre what suggests that the surrounding material of PMS stars in the cluster centre, that usually should produce H_α emission, has already been swept away by the powerful radiation field of the most massive stars. Such a possibility has been suggested for explaining the lack of emission stars in NGC 6231 (Sung et al. 1998) and in Upper Scorpius OB Association (Preibisch & Zinnecker 1999). If this is true, the rest of PMS included in the cluster area should be weak–lined PMS stars only detectable as X–ray emitters (Montmerle 1996).

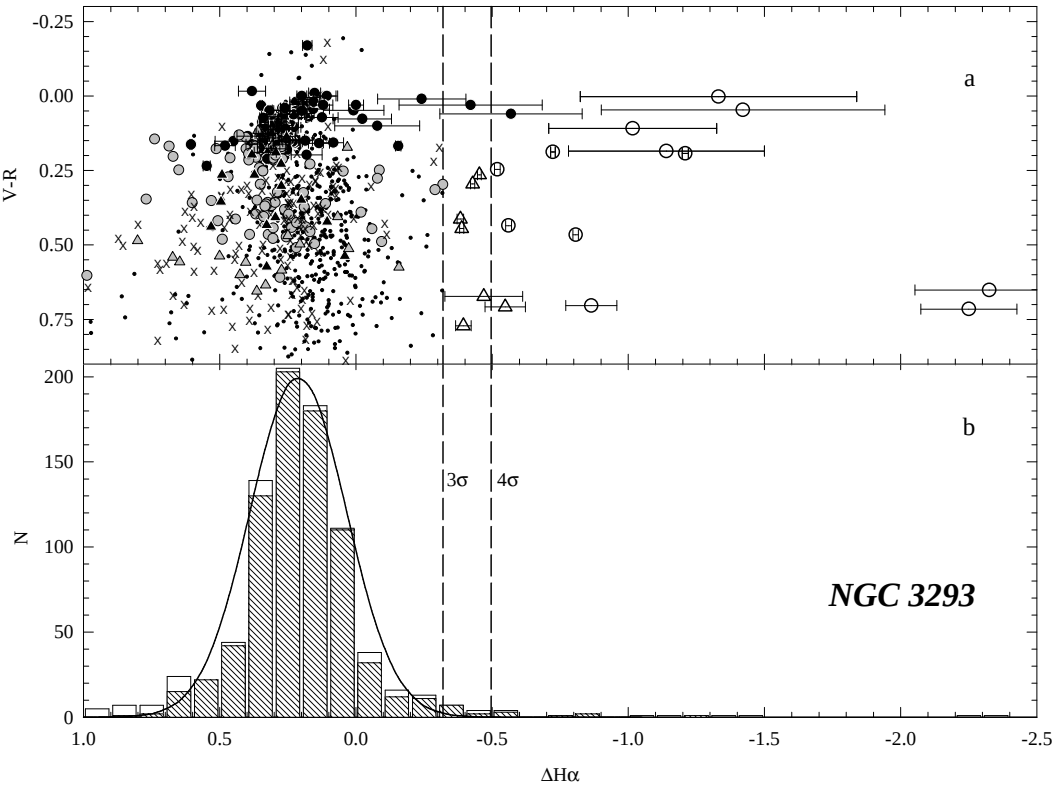

Fig. 11. **a)** $V - R$ vs. $\Delta\ H_\alpha$ diagram. Symbols as in Fig 2a. Error bars from DAOPHOT task for 'lm1' and H_α emission stars are also indicated. **b)** $\Delta\ H_\alpha$ distribution. White histogram corresponds to all stars with $\Delta\ H_\alpha$ index and the hatched one only includes those with index errors < 0.1. Solid curve is a Gaussian distribution function fitted to dashed histogram (see section 5). Dashed lines are 3σ and 4σ limits for H_α emission stars selection.

6. Discussion

Uncertainties in the memberships and also in the stellar age assignment make difficult the interpretation of the star formation process in an open cluster. These uncertainties can lead to a wrong estimate of the star formation rate and therefore to a misinterpretation of the entire process. We attempted to reduce such uncertainties by verifying the reliability of the field star sample used to remove the contribution of field stars and proving that no mass segregation is present in NGC 3293. Moreover, when removing the field contribution from the CMDs of NGC 3293 we chose limits which define the PMS band in terms of both, extension and wide at a high level of credibility so that only a few stars must have been lost by this procedure. So, we do not expect our conclusions are seriously affected (qualitatively speaking).

As noticed above, the lack of coincidence between the mean stellar distribution of PMS stars and a given isochrone has been historically used as evidence against the coeval hypothesis (Iben & Talbot 1966); in the present case there is a strong coincidence. There is a 2 Myr difference between the mean nuclear age and the mean contraction age, but it can be explained in terms of the various effects already mentioned. There is no chance either that the age difference between massive and PMS stars reaches the high value of 20 Myr indicated by HM82. That stars in NGC 3293 were all formed in a short period of time is additionally supported by the "turn–on" mass location at $\sim 2\mathcal{M}_\odot$ (compatible with a contraction time ranging from 6 to 12 Myr) and by the most evolved star in the cluster, the red super–giant, which is $10 - 12$ Myr old, thus equalising the mean age of PMS stars.

The computation of the SFR confirms the above suggestions in the sense that no total increasing SFR, as proposed in other clusters (e.g. NGC 6530 and NGC 2264, Iben & Talbot 1966) is evident in NGC 3293. Indeed, the picture of this cluster could be similar to the re–interpretation of NGC 2264 and 6530 data (from Iben & Talbot 1966) made by Stahler (1985). This author found no obvious mass–age correlation but that the star formation in these two clusters took place in a period of time from 5 to 12 Myr. A similar results has been reported for the Upper Scorpius OB Association (Preibisch & Zinnecker 1999; Preibisch et al. 2002) and for the Scorpius–Centaurus OB Association (Mamajek et al. 2002) where was not found either evidences for a real age spread among PMS stars as the stellar formation proceeded during a short but intense burst of a few millions years, probably triggered by a supernova event.

Table 5. Likely and probable H_α emission stars.

Likely H_α emission stars.										
#	$\#_T$	$\#_{HM}$	X	Y	V	$U-B$	$B-V$	$V-R$	$V-I$	$\Delta\ H_\alpha$
31	28	-	199.7	340.9	10.27	-0.66	0.01	0.00	0.05	-1.33 ::
63	-	277	196.9	85.5	12.02	-0.28	0.22	0.18	0.39	-1.14 ::
67	117	-	124.6	570.0	12.10	-0.38 :	0.28	0.05	0.44	-1.42 ::
85	-	264	208.8	170.1	12.34	-0.48	0.10	0.11	0.23	-1.02 ::
297	-	287	506.0	130.0	14.56	0.20	0.31	0.19	0.43	-0.72
324	-	286	546.9	125.0	14.69	0.25	0.31	0.19	0.42	-1.21
361	-	-	236.4	702.4	14.93	.	.	0.25	.	-0.52
397	-	288	487.3	131.0	15.22	0.40	0.77	0.47	0.87	-0.81
438	-	275	312.3	64.0	15.45	0.22	0.70	0.43	0.86	-0.56
819	-	-	816.0	195.5	17.15	.	.	0.72	.	-2.25 ::
989	-	-	602.4	765.1	17.72	.	.	0.65	.	-2.33 ::
1544	-	-	771.5	519.2	19.62	.	.	0.70	.	-0.86 :
Probable H_α emission stars.										
#	$\#_T$	$\#_{HM}$	X	Y	V	$U-B$	$B-V$	$V-R$	$V-I$	$\Delta\ H_\alpha$
271	-	-	285.0	722.4	14.40	.	.	0.26	.	-0.45
391	-	-	351.9	723.8	15.16	.	.	0.44	.	-0.39
458	-	-	147.0	665.3	15.58	0.13 :	0.72 :	0.30	0.80 :	-0.43
648	-	-	170.2	663.8	16.47	0.46 :	0.87 :	0.41	0.97 :	-0.38
926	-	-	323.4	91.2	17.52	0.95 ::	1.28	0.77	1.50	-0.39
1448	-	-	667.3	722.6	19.20	.	.	0.71	.	-0.55 :
1599	-	-	634.7	748.2	19.93 :	.	.	0.67 :	.	-0.47 ::

Notes: -$\#_T$ and $\#_{HM}$ means star numbers from TGHH80 and HM82 respectively.
-Colon (:) and double colon (::) indicate data with errors larger than 0.04 and 0.10 respectively.

7. Conclusions

We have investigated the open cluster NGC 3293 area with deep broad band and H_α photometry obtaining a picture of its main sequence structure down to $M_V \approx +4.5$. The picture demonstrates that the upper part of its sequence is composed by stars evolving off the ZAMS, the mid one mostly includes stars on the ZAMS yet and the lower main sequence consists of stars that are placed above the ZAMS becoming a PMS population.

Clear indications confirming the existence of a PMS population in this cluster are presented after a very careful removal of the field star contamination and also from the finding of H_α emission stars. Our analysis yielded that NGC 3293 is placed at a distance $d = 2750\ pc$ and has a $4'.1$ angular radius ($3.3\ pc$). The absorption law affecting the cluster is normal although it is close to the northern part of the HII region NGC 3372. In this last particular place, abnormal extinction laws have been found (e.g. Vázquez et al. 1996; Tapia et al. 2002; Carraro et al. 2002). Following the common pattern of clusters in this galactic region, NGC 3293 shows, however, differential reddening surely produced by intracluster material.

Superposition of modern isochrones indicates this object has a nuclear age of 8 Myr and almost a similar mean value of 10 Myr was found among its faintest, PMS, stars. Therefore, the star formation in NGC 3293 appears to be coeval. Hints that star formation still continues (although at a probably low rate) in NGC 3293 is given by the detection of stars showing H_α emission. These stars are not concentrated towards the cluster centre but they tend to lie in the cluster periphery determined by star counts. The most likely explanation for this lack of concentration may be found in the fact that the radiation field of massive stars has swept away the material that surrounds the PMS stars.

The computation of the cluster LF did not show the strong dip in its structure nor the halo structure of faint stars, as previously suggested by HM82. As many other young clusters (Tr 14, Vázquez et al. 1996; NGC 6231, Baume et al. 1999; or Pismis 20, Vázquez et al. 1995) we found that the IMF of NGC 3293 has a slope value $x = 1.2 \pm 0.2$. This value is of the same order than the one found by Massey et al. (1995) who investigated many open clusters and associations in the Galaxy, the LMC and the SMC finding a mean slope values of 1.1 ± 0.1.

This article is partially based in the Digitized Sky Survey that was produced at the Space Telescope Science Institute under US government grant NAG W-2166. Original plate material is copyright the Royal Observatory Edinburgh and the Anglo–Australian Observatory. This research, also, has made use of the SIMBAD database, operated at CDS, Strasbourg, France.

Acknowledgements. The authors acknowledge the financial support from the Facultad de Ciencias Astronómicas y Geofísicas de La UNLP and the IALP–CONICET. Special thanks are given to Dr. Garrison for the allocation of telescope time at UTSO and to the CASLEO staff for the technical support. G.B. gratefully acknowledges the collaboration of the Università di Padova (Italy) during a postdoctoral grant.

References

Abt H.A., 1979, ApJ 230, 485
Adams M.T., Strom K.M., & Strom S.E., 1983, ApJS 53, 893
Balona L.A. & Crampton D., 1974, MNRAS 166, 203
Balona L.A., 1975, MmRAS 78, 51
Balona L.A., 1994, MNRAS 267, 1060
Balona L.A. & Engelbrecht C., 1981. Workshop on Pulsating B stars, p. 195. Eds. G.V.O.N. & C. Sterken, Nice Observatory
Balona L.A. & Engelbrecht C., 1983, MNRAS 202, 293
Baume G., Paoli S., Vázquez R.A., & Feinstein A., 1994, RMxAA 29, 212
Baume G., 1999, Ph.D. thesis, Universidad Nacional de La Plata
Baume G., Vázquez R.A., & Feinstein A., 1999, A&A 137, 233
Battinelli P., Capuzzo–Dolcetta R., & Nesci R., 1991, MemSAIt 62, 915
Bernasconi P.A. & Maeder A., 1996, A&A 307, 829
Bessell M.S. & Stringfellow G.S., 1993, ARA&A 31, 433
Carraro G., 2002, MNRAS 331, 785
Carraro G., Ventura P., Romanielo M., & Patat F., 2002, (submitted to A&A)
Conti P.S. & Underhill A.B., 1988, In "O stars, & Wolf–Rayet stars", Monograph Series of non–thermal phenomena in stellar atmospheres, CNRS and NASA, Conti P.S. and Underhill A.B. (eds.)
Cousins, A.W.J., 1978, MNSSA 37, 62
Chen B., Carraro G., Torra J., & Jordi C., 1998, A&A 331, 916
de Bruijne J.H.J., Hoogerwerf R. & de Zeeuw P.T., 2000, ApJ 544, L65
Dean J.F., Warren P.R., & Cousins A.W.J., 1978, MNRAS 183, 569
Deeg H.J. & Ninkov Z., 1996, A&AS 119, 221
ESA, 1997, The Hipparcos and Tycho Catalogues, ESA SP-1200
Feast M.W. 1958, MNRAS 118, 618
Feinstein A. & Marraco H.G., 1980, PASP 92, 266
Flaccomio E., Micela G., Sciortino S., & Favata F., Corbally C., & Tomaney A., 1999, A&A 345, 521
Forbes D., 1996, AJ 112, 1073
Girardi L., Bressan A., Bertelli G., & Chiosi C., 2000, A&AS 141, 371
Hartigan P., Strom K.M., & Strom S.E., 1994, ApJ 427, 961
Herbst W. & Miller D.P., 1982, AJ 87, 1478
Hillenbrand L.A., Massey P., Strom S.E., & Merrill K. M., 1993, AJ 106, 1906
Iben I. & Talbot R.J., 1966, ApJ 144, 968
Janes K.A., Tilley C., & LingåG., 1988, AJ 95, 771
Kenyon S.J. & Hartmann L.W., 1990, ApJ 349, 197
Kroupa P., Tout C.A. & Gilmore G., 1991, MNRAS 251, 293
Kroupa P., Gilmore, G. & Tout C.A., 1992, AJ 103, 1602
Kroupa P. & Tout C.A., 1992, MNRAS 259, 223
Lada C.J., Margulis M. & Deaborn D., 1984, ApJ 285, 141
Lada E.A., Strom K.M. & Meyers P.C., 1993, in Prototstars and Planets III, edited by E.H. Levy and J.I. Lunine (University of Arizona Press, Tucson), p. 245
Lada E .A. & Lada C.J., 1995, AJ 109, 1682
Landolt, A.U., 1992, AJ 104, 340
Mamajek E.E., Meyer M.R., & Liebert J., 2002, AJ 124, 1670
Massey P., Johnson K.E., & DeGioia–Eastwood K., 1995, ApJ 454, 151
Meynet G., Mermilliod J.-C., & Maeder A., 1993, A&AS 98, 477
Mermilliod J.-C., 1976, A&A 53, 289
Montmerle, T., 1996, in ASP Conf. Ser. 109, Ninth Cambridge Workshop on Cool Stars, Stellar Systems, and the Sun, ed. R. Pallavicini & A.K. Dupree (San Francisco: ASP), 405
Patat F. & Carraro G., 2001, MNRAS 325, 1591
Phelps R.L. & Janes K.A., 1993, AJ 106, 1870
Preibisch T. & Zinnecker H., 1999, AJ 117, 2381
Preibisch T., Brown A.G.A., Bridges, T., Guenther E., & Zinnecker H., 2002, AJ 124, 404
Prisinzano L., Carraro G., Piotto G., Seleznev A.F., Stetson P.B., & Saviane I., 2001, A&A 369, 851
Rachford B.J. & Canterna R., 2000, AJ 119, 1296
Sagar R. & Richtler T., 1991, A&A250, 324
Sanner J. & Geffert M., 2001, A&A 370, 87
Scalo J, 1986, Fund. Cos. Phys. 11, 1
Schild R.E., 1970, ApJ 161, 855
Schmidt–Kaler Th., 1982, in Landolt–Bornstein VI/2b
Shobbrook R.R., 1980, MNRAS 192, 821
Shobbrook R.R., 1983, MNRAS 205, 1215
Stahler S.W., 1985, ApJ 293, 207
Stahler S.W. & Fletcher A.B., 1991, MemSAIt 62, 767
Stetson P.B., 1987, PASP 99, 191
Sung H., Bessell M.S., & Lee S.-W., 1998, AJ 115, 734
Tapia M., Roth M., Vázquez R. A., & Feinstein A., 2002, (submitted to MNRAS)
Turner D.G., Grieve G.R., Herbst W., & Harris W.E., 1980, AJ 85, 1193
van den Bergh S. & Sher D., 1960, Pub. of the DDO 2, 203
Vázquez R.A. & Feinstein A., 1991, A&AS 90, 317
Vázquez R.A., Baume G., Feinstein A., & Prado P., 1994, A&AS 106, 339
Vázquez R.A., Will J.-M., Prado P., & Feinstein A., 1995, A&AS 111, 85
Vázquez R.A., Baume G., Feinstein A., & Prado P., 1996, A&AS 116, 75
Vázquez R.A., Baume G., Feinstein A., & Prado P., 1997, A&AS 124, 13
Vázquez R.A. & Baume G., 2001, A&A 371, 908
Walker M.F., 1957, ApJ 125, 636
Walker M.F., 1961, ApJ 133, 438
Wilner D.J. & Lada C.J., 1991, AJ 102, 1050